Enhanced second-harmonic generation in high-Q all-dielectric metasurfaces with backward frequency conversion

Xu Tu [1,2] Siqi Feng, [1,2] Jiajun Li, [1,2] Yangguang Xing, [1,2] Feng Wu [3] Tingting Liu [1,2,*] and Shuyuan Xiao [1,2,†]

[1] *School of Information Engineering, Nanchang University, Nanchang 330031, China*

[2] *Institute for Advanced Study, Nanchang University, Nanchang 330031, China*

[3] *School of Optoelectronic Engineering, Guangdong Polytechnic Normal University, Guangzhou 510665, China*

(Received 1 May 2024; accepted 12 June 2024; published 27 June 2024)

Here we employ the quasibound state in the continuum (quasi-BIC) resonance in all-dielectric metasurfaces for efficient nonlinear processes in consideration of the backward frequency conversion. We theoretically study second-harmonic generation (SHG) from symmetry-broken AlGaAs metasurfaces and reveal the efficiency enhancement empowered by high-Q quasi-BIC resonances. By introducing the correction term of nonlinear polarization at the fundamental wave field to the conventional undepleted approximation, we uncover the effect of backward frequency conversion on the nonlinear conversation efficiency. The SHG efficiency of 2.45×10^{-2} with the developed depleted model shows a 14.3% decrease compared with 2.86×10^{-2} in the conventional undepleted approximation, under an incident intensity of 10 MW/cm^2. Our results are of importance for designing efficient nonlinear metasurfaces supporting high-Q resonances.

DOI: 10.1103/PhysRevA.109.063522

I. INTRODUCTION

Frequency conversion processes, which involve the interaction between intense light and matter, have made considerable advancements following the development of lasers [1]. Harmonic generation processes such as second- (SHG) and third-harmonic generation (THG) are the most fundamental physical phenomena in nonlinear optics, and they have attracted growing interest with regard to a large variety of optical devices. They are traditionally realized in bulk nonlinear crystals, where the cumbersome phase-matching condition is required to satisfy momentum match for efficient frequency conversion. The typical bulk size and the phase-matching constraint are incompatible with advanced technologies. In recent years, advances in nanofabrication techniques have revolutionized the framework of nonlinear processes. Ultrathin metasurfaces hold great promise for replacing bulk crystals because they can relax the phase-matching constraint and simultaneously manipulate nonlinear fields with favorable conversion efficiencies [2,3]. For example, plasmonic metasurfaces were first used in harmonic generation, frequency mixing, and other nonlinear effects [4,5]. Because the plasmonic mechanism relies on the collective oscillation of free electrons, the inevitable Ohmic loss and heat effect would lead to a low threshold for optical damage. These shortcomings in metallic nanoresonators inherently limit the nonlinear conversion efficiency and hinder their applicability in nonlinear nanophotonic devices.

Recently, all-dielectric metasurfaces have been demonstrated to enhance and manipulate nonlinear frequency conversation processes at the nanoscale [6–8]. In addition to the advantages of the low loss, high refractive index, and high damage threshold, they exhibit multipolar characteristics with the coexistence of electric and magnetic resonant modes known as Mie-type resonances, giving rise to the strong localization of electromagnetic fields beneficial for high nonlinear conversation efficiency. In particular, bound states in the continuum (BICs) in all-dielectric metasurfaces have been proven to be a promising way to achieve higher efficiencies of nonlinear optical processes by engineering radiation leakage. When the radiation channel is opened, sharp quasi-BIC resonances with high-quality factors (Q factors) are formed accompanied by strong local field enhancement [9,10]. It was reported that such high-Q quasi-BIC resonances can boost substantially nonlinear frequency conversion processes in dielectric metasurfaces such as SHG [11–14], THG [15–17], high-harmonic generation (HHG) [18–21], sum-frequency generation (SFG) [22–25], and four-wave mixing (FWM) [26–29]. Indeed, the quest for high conversion efficiency is rooted in the enhancement of a local field inside nonlinear nanostructures. Conventionally, the nonlinear frequency conversion process is simply attributed to the forward frequency conversion of fundamental waves to nonlinear waves. However, when the local field is large enough, the influence of backward coupling, i.e., the backward frequency conversion of nonlinear waves to fundamental waves, cannot be ignored.

In this work, we study the efficient nonlinear SHG process in quasi-BIC dielectric metasurfaces in consideration of backward frequency conversion. We apply the approach as a depleted model to nonlinear AlGaAs metasurfaces where the excitation of quasi-BIC resonance allows for extremely enhanced local fields, leading to the high efficiency of the SHG process. We show that the conversion efficiency of SHG becomes lower in quasi-BIC dielectric metasurfaces when the

*Contact author: ttliu@ncu.edu.cn

†Contact author: syxiao@ncu.edu.cn

 ©2024 American Physical Society

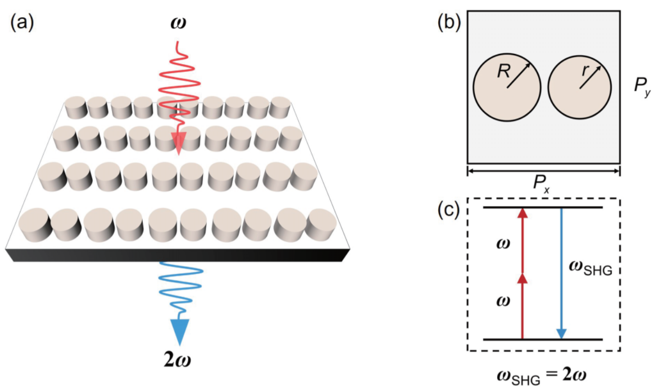

FIG. 1. (a) The conceptual schematic of the SHG process in the quasi-BIC metasurfaces. (b) The planar portion of the unit cell. Geometric parameters: the period is $p_x = p_y = 1020$ nm, the height is $h = 300$ nm, and the radii are initially set to $R = r = 225$ nm. (c) The energy diagram of the SHG process.

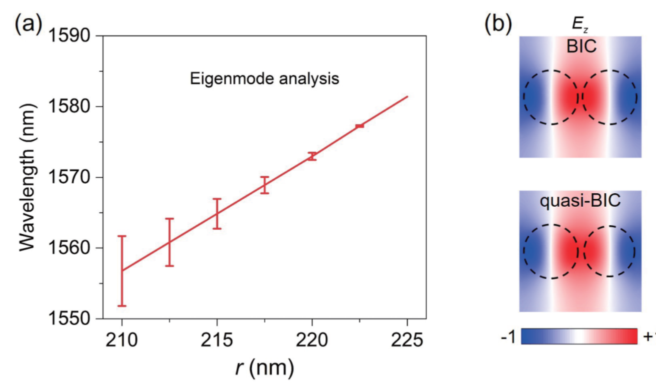

FIG. 2. (a) The eigenmode of the quasi-BIC metasurfaces as a function of the pump wavelength and the radius r. The error bars represent the relative magnitude of the mode inverse radiation lifetime. (b) The distribution of magnetic fields in the z-direction E_z for both BIC and quasi-BIC.

backward frequency conversion is taken into account in the form of the correction term of nonlinear polarization at the fundamental wave field. In the designed metasurface, consideration of the backward frequency conversion combined with the forward frequency conversion is necessary with a pump intensity of 10 MW/cm^2 where the difference in SHG efficiency calculated based on the undepleted and depleted models approaches 14.3%.

II. HIGH-Q QUASI-BIC RESONANCE IN AlGaAs METASURFACES

We consider the resonant AlGaAs metasurfaces for the nonlinear SHG process, as shown in Fig. 1. The fundamental pump wave is normally incident to the metasurface structure, and the transmitted SHG signals are collected from the substrate side. AlGaAs is chosen because of its strong second-order nonlinear susceptibility for SHG response and for its high refractive index, which is necessary to sustain the quasi-BIC resonances in the wavelength of interest [30,31]. The metasurfaces are composed of a square lattice of patterned AlGaAs nanodisks of height $h = 300$ nm on top of a SiO_2 substrate with a period of $p_x = p_y = 1020$ nm. The refractive index of AlGaAs is derived from experimental data and plotted in Fig. S1 [32] (see also Ref. [33] therein), and the refractive index of the substrate is set to 1.45. The radii of circular-circular nanodisks are $R = r = 225$ nm. A tunable geometrical parameter here is the radius r of the nanodisk at the right side.

We start from the eigenmode analysis to calculate and optimize the resonant mode of the metasurface system using the finite-element method via COMSOL MULTIPHYSICS. The metasurfaces are considered as an infinite structure with perfect periodicity. Figure 2(a) shows the resonant modes of the structure as a function of the geometrical parameter of the radius r. The error bars represent the relative magnitude of the mode inverse radiation lifetime, i.e., radiation loss γ. Here we would like to use the relative length of the error bars to more intuitively characterize the increase of the BIC eigenmode inverse radiation lifetime with the structural symmetry breaking. In other words, we do not focus on the specific unit but rather on the relative length of the error bars. The lengths of error bars are normalized via multiplying them by a constant coefficient. The eigenfrequency values, including the real and imaginary parts, are listed in Table S1 [32]. It is observed that the variations of r change the eigenfrequency and radiation loss of the system. At $r = R = 225$ nm, the metasurfaces support a symmetry-protected BIC that is completely decoupled from the external free space as a nonradiative mode with $\gamma = 0$. To transform the symmetry-protected BIC into a leaky mode, we break the structural symmetry by changing r to provide a certain radiation leakage channel. Thus, as r deviates from 225 nm, the genuine BIC is transformed into the quasi-BIC with increasing radiation loss. This evolution can also be validated by the electric field distributions E_z in Fig. 2(b), where the in-plane inversion symmetry $(x, y) \rightarrow (-x, -y)$ of E_z at BIC is slightly broken by the structural perturbation.

We proceed to the linear response of the metasurfaces under the normally incident x-polarized plane wave. Figure 3(a) depicts the transmission spectra with varying radius r. When the structure is symmetric with $r = R = 225$ nm, the transmission spectra display a disappearing dip that broadens as r becomes smaller. This reveals that the BIC with an infinite Q factor transforms into finite-Q quasi-BIC, which confirms the results of the eigenmode analysis. As shown in Fig. 3(b), the Q factor exhibits a quadratic dependence on the asymmetric parameter α defined as $\alpha = 1 - r^2/R^2$, i.e., $Q \propto \alpha^{-2}$. Such universal behavior for the Q factor of a quasi-BIC remains valid for the proposed symmetry-broken metasurfaces [34–36]. We provide the transmission spectrum for the metasurfaces with $r = 220$ nm in Fig. 3(c). The asymmetric Fano shape is observed with the resonant wavelength at 1572.95 nm. According to the coupled-mode theory [16,37,38], the Q factor can be calculated by $\omega_0/2\gamma$ as 8950, indicating the remarkably confined field of the leaky quasi-BIC, with the strong field enhanced by a factor 110. Furthermore, the multipolar decomposition results in Fig. 3(d) reveal that the toroidal dipole plays the dominate role in this quasi-BIC resonance. The expressions of multipolar decomposition can be found in the Supplemental Material [32]; see also Refs. [39,40] therein.

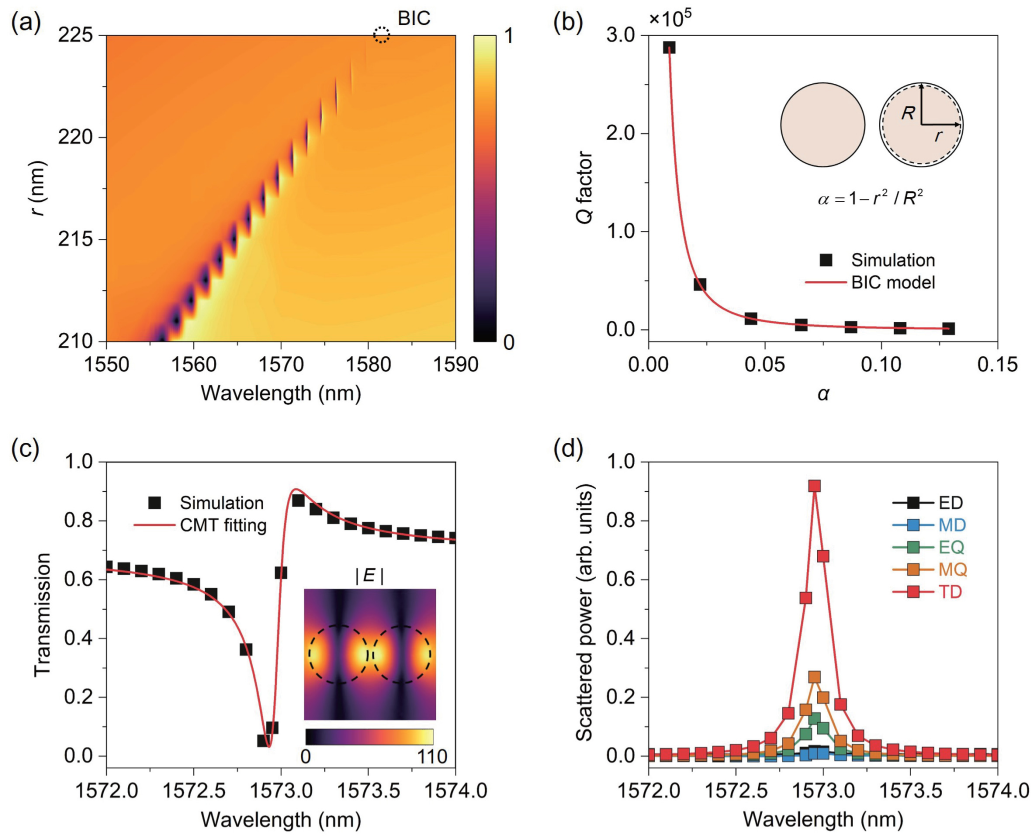

FIG. 3. (a) The transmission spectra of the quasi-BIC metasurfaces as a function of wavelength and radius r. (b) The quadratic dependence of the Q factor on the asymmetry parameter α. (c) The simulated and theoretically fitted transmission spectrum for the quasi-BIC metasurface with $r = 220$ nm. The inset shows the distribution of the electric field in the x-y plane at the corresponding resonant wavelength. (d) The multipolar decomposition of scattered power for the metasurface with $r = 220$ nm.

III. RESONANTLY ENHANCED SHG WITH BACKWARD FREQUENCY CONVERSION

We come now to the quasi-BIC enhanced nonlinear response of the metasurfaces. The coupling wave equation at the fundamental and harmonic wavelength is written as [41]

$$\nabla^2 \vec{E} - \frac{1}{c^2}\frac{\partial^2 \vec{E}}{\partial t^2} = \mu_0 \frac{\partial^2 \vec{P}_{\rm nl}}{\partial t^2}, \tag{1}$$

where $c = c_0/n$, $n = 1 + \chi$, $c_0 = 1/\sqrt{\varepsilon_0 \mu_0}$ is the speed of light in vacuum, χ is the linear polarizability, $\vec{E}$ is the electric field generated by the nonlinear polarization source, and $P_{\rm nl}$ is the nonlinear polarization. When only forward frequency conversion is considered, $P_{\rm nl}$ can be conventionally represented by the nonlinear polarization at the SH wavelength $P_{\rm nl}^{(2\omega)}$. For noncentrosymmetric materials such as AlGaAs adopted herein, the induced nonlinear polarization for the SHG process is

$$\vec{P}^{(2\omega)} = \varepsilon_0 \chi^{(2)} \vec{E}^{(\omega)} \vec{E}^{(\omega)}, \tag{2}$$

where ε_0 is the vacuum dielectric constant with 8.8542×10^{-12} F/m, and $\chi^{(2)}$ is the second-order polarizability electric field inside the material. For AlGaAs material, only off-diagonal elements of the tensor χ^2 are nonzero, i.e., $\chi_{ijk}^{(2)} = \chi^{(2)} = 100\,\mathrm{pm/V}$, $i \neq j \neq k$. Therefore, Eq. (2) can be explicitly written as

$$\begin{bmatrix} P_x^{(2\omega)} \\ P_y^{(2\omega)} \\ P_z^{(2\omega)} \end{bmatrix} = 2\varepsilon_0 \chi^{(2)} \begin{bmatrix} E_y^{(\omega)} E_z^{(\omega)} \\ E_x^{(\omega)} E_z^{(\omega)} \\ E_x^{(\omega)} E_y^{(\omega)} \end{bmatrix}. \tag{3}$$

Based on Eq. (3), only forward frequency conversion is considered. The nonlinear simulations of the SHG process are implemented with the conventional undepleted pump approximation using two typical steps. First, the linear response at the fundamental wavelength is calculated for the local field distributions, and the nonlinear polarization inside the meta-atom is induced. Second, the polarization term is employed as the only source to excite the electromagnetic field at the harmonic wavelength to generate SH radiation.

In the case of highly efficient frequency conversion, the electric field amplitudes inside the nonlinear meta-atoms at the fundamental and SH wavelengths may be comparable. When considering SHG as a degenerate three-wave-mixing process, the forward frequency conversion ($\omega + \omega \rightarrow 2\omega$) process and the backward frequency conversion ($2\omega + \omega^* \rightarrow \omega$) processes are equally important in frequency conversion. Instead of the above undepleted approximation, the depleted model, taking into account forward and backward frequency conversions, should be exploited in this case. Since the coupling of nonlinear waves to fundamental waves could not be neglected, $P_{\rm nl}$ should include nonlinear polarization at the

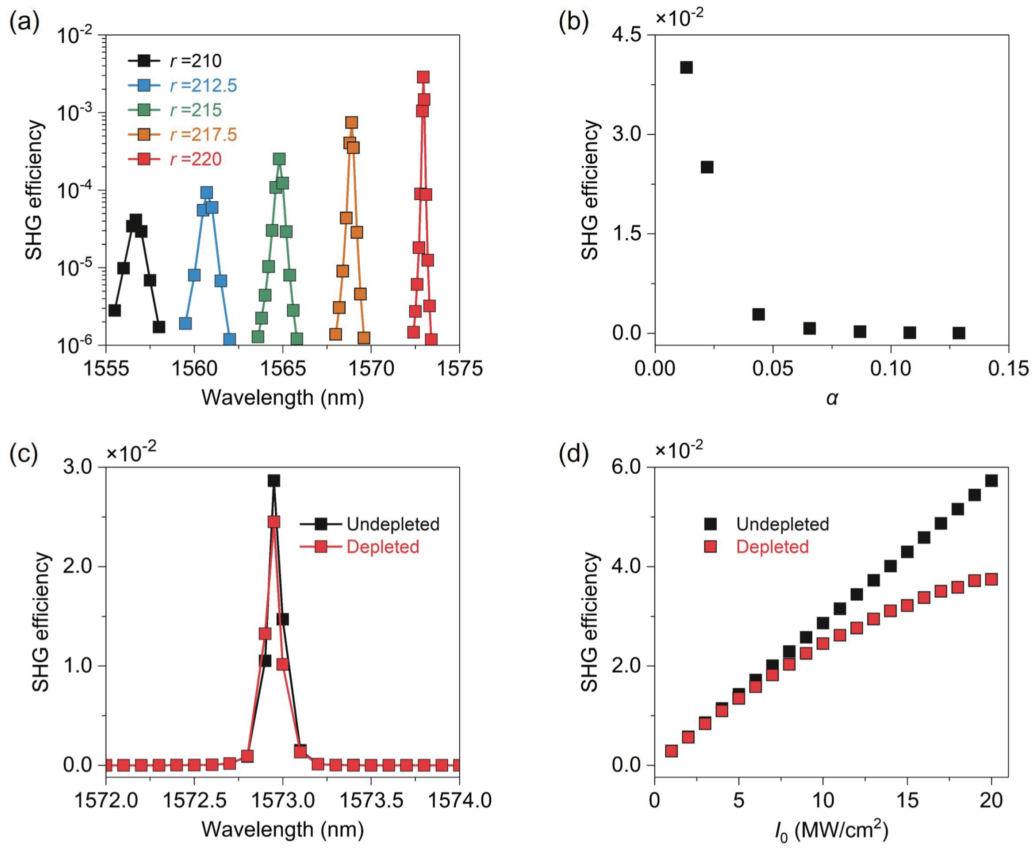

FIG. 4. (a) The SHG conversion efficiencies with undepleted approximation in the quasi-BIC metasurfaces with the radius ranging from $r = 210$ to 220 nm under an incident pump intensity of 1 $\mathrm{MW/cm^2}$. (b) The dependence of SHG efficiency on the asymmetry parameter α. (c) The comparison of the SHG efficiencies with undepleted and depleted approximations in the quasi-BIC metasurface with $r = 220$ nm under an incident pump intensity of 10 $\mathrm{MW/cm^2}$. (d) The SHG efficiencies with undepleted and depleted approximations as a function of the incident pump intensity.

SH wavelength $P_{\mathrm{nl}}^{(2\omega)}$ and the correction term of nonlinear polarization at the fundamental wavelength $P_{\mathrm{nl}}^{(\omega)}$, i.e., $P_{\mathrm{nl}} = P_{\mathrm{nl}}^{(\omega)} + P_{\mathrm{nl}}^{(2\omega)}$. In a principal crystalline axis system such as the AlGaAs material, the nonlinear source $P_{\mathrm{nl}}^{(2\omega)}$ at the SH wavelength is given by Eq. (3), and the expression for $P_{\mathrm{nl}}^{(\omega)}$ at the fundamental wavelength takes the form [42]

$$\begin{bmatrix} P_x^{(\omega)} \\ P_y^{(\omega)} \\ P_z^{(\omega)} \end{bmatrix} = 2\varepsilon_0 \chi^{(2)} \begin{bmatrix} E_y^{(2\omega)} E_z^{(\omega)*} + E_z^{(2\omega)} E_y^{(\omega)*} \\ E_x^{(2\omega)} E_z^{(\omega)*} + E_z^{(2\omega)} E_x^{(\omega)*} \\ E_x^{(2\omega)} E_y^{(\omega)*} + E_y^{(2\omega)} E_x^{(\omega)*} \end{bmatrix}. \quad (4)$$

In the depleted approximation model, the simulation for the nonlinear SHG process follows two steps. After the first step, in which the linear response is computed at the fundamental wavelength, the second step for nonlinear response considers both the nonlinear polarizations $P_{\mathrm{nl}}^{(\omega)}$ and $P_{\mathrm{nl}}^{(2\omega)}$ as sources in the fundamental and second-harmonic frequencies, respectively, to excite the electromagnetic response that radiates the SHG signal. More details about the modeling methodology of nonlinear simulations can be found in the Supplemental Material [32].

We first calculate the SHG efficiency with the undepleted pump approximation under different asymmetric geometrical parameters of the metasurface. In simulations, the incident light intensity is set to 1 $\mathrm{MW/cm^2}$. The conversion efficiency of SHG is defined by $\eta_{\mathrm{SH}} = P_{\mathrm{SH}}/P_{\mathrm{FF}}$, where P_{SH} is the radiative power of the transmitted SH signal collected from the substrate side, and P_{FF} is the incident pump power at the fundamental wavelength. In Fig. 4(a), the conversion efficiency of SHG, η_{SH}, increases with the increase of the radius r in the quasi-BIC metasurface. For the proposed metasurface with $r = 220$ nm, SHG efficiency is comparable or even better than previous theoretical results with quasi-BIC enhanced second-order nonlinear processes [12,13,43,44]. Given that the geometric asymmetry is related to the Q factor of quasi-BIC resonance and the field confinement performance, we further explore the dependence of the SHG efficiency on the asymmetric parameters α. It is observed in Fig. 4(b) that η_{SH} is subject to α, which is consistent with the quadratic dependence of the Q factor on α. As the asymmetric parameter increases, the radiation loss of the system increases, leading to the dramatic decline of the Q factor and electric field energy. As a result, the conversion efficiency of the SHG process decreases significantly.

We further take into consideration the backward frequency conversion of the SH radiation field on the fundamental wave field. The SHG conversion efficiency is calculated with the depleted approximation in the quasi-BIC metasurface with $r = 220$ nm. To clearly observe the effect of the backward frequency conversion, the incident pump is increased to 10 $\mathrm{MW/cm^2}$. With the undepleted and depleted approximations, the SHG efficiencies are compared in Fig. 4(c). Both efficiency curves display significant enhancement at the resonant wavelength due to the high-Q quasi-BIC resonance. The peak efficiency with the undepleted approximation is calculated as 2.86×10^{-2}, higher than that with the depleted model of 2.45×10^{-2}. The undepleted approximation causes error above 14.3% in nonlinear simulations. This means that the system no longer completely satisfies the conditions for the undepleted approximation due to the high enough SHG efficiency for the SH field comparable to the fundamental field. It is estimated that the nonlinear polarization $P_{\mathrm{nl}}^{(\omega)}$ at the fundamental frequency cannot be ignored at high pump intensity.

In Fig. 4(d), we finally explore the dependence of the SHG efficiency on the incident pump intensity. The SHG conversion efficiency with the undepleted approximation is proportional to the light intensity. This implies that the nonlinear SHG efficiency can be enhanced by orders of magnitude by increasing the input light intensity. However, it is not feasible in practice when the backward frequency conversion is taken into account. With the backward frequency conversion of the SH radiation field on the fundamental field, the SHG efficiency would not increase linearly, but it would reach saturation as the pump intensity further increases, as shown in Fig. 4(d). In the proposed metasurface, the SHG efficiency is 3.74×10^{-2} at a pump intensity of 20 $\mathrm{MW/cm^2}$ when the backward frequency conversion is considered, much smaller than the efficiency of 5.73×10^{-2} with the undepleted approximation. This backward frequency conversion would be observable when implementing very high pump intensity [19,21,45,46]. It is noticed that the irreversible damage of the nonlinear material AlGaAs may occur at a very high incident pump intensity due to the increased absorption enhanced by the resonantly enhanced local electric field. Previous experiments have reported that the damage threshold for the incident peak intensity is approximately several $\mathrm{GW/cm^2}$. Specifically, the damage threshold I_{d} is determined by two factors: (i) the intensity of the incident pump I, and (ii) the enhancement of the local electric field f, which can be expressed by a simple relation $I_{\mathrm{d}} = f^2 I$. Considering the experimentally estimated values of $f_1^2 = 30$ and $I_1 = 8.1$ $\mathrm{GW/cm^2}$ [47,48], and the theoretically calculated $f_2 = 110$ that can be observed from the inset in Fig. 3(c), the threshold of incident intensity can be obtained as $I_2 = 20.1$ $\mathrm{MW/cm^2}$. Therefore, we would end with a maximum incident pump intensity <20 $\mathrm{MW/cm^2}$ in Fig. 4(d).

IV. CONCLUSIONS

In conclusion, we demonstrate the efficient nonlinear SHG process in quasi-BIC dielectric metasurfaces. For the proposed engineered asymmetric AlGaAs metasurfaces, the SHG conversion efficiency can be enhanced up to 10^{-2} orders of magnitude under an incident intensity of 10 $\mathrm{MW/cm^2}$. When taking the backward frequency conversion into consideration by introducing the correction term of nonlinear polarization at the fundamental wave field, we find that the conversion efficiency calculated by the developed depleted model becomes lower, with around a 14.3% decrease compared with that with the conventional undepleted approximation. Our calculation results are based on the general coupled wave equation through considering SHG as a degenerate three-wave mixing process, and they would be in more agreement with actual circumstances. A similar approach can be applied to the case of SHG from other III-V semiconductor metasurfaces, where either ultrahigh-Q resonances or sufficiently strong pump power is exploited. Thus, our general approach is of importance for designing efficient nonlinear metasurfaces supporting high-Q resonances toward high-efficiency frequency conversion, optical switching, and modulation.

ACKNOWLEDGMENTS

This work was supported by the National Natural Science Foundation of China (Grants No. 12304420, No. 12264028, No. 12364045, and No. 12104105), the Natural Science Foundation of Jiangxi Province (Grants No. 20232BAB201040 and No. 20232BAB211025), the Guangdong Basic and Applied Basic Research Foundation (Grant No. 2023A1515011024), the Young Elite Scientists Sponsorship Program by JXAST (Grant No. 2023QT11), and the Innovation Fund for Graduate Students of Jiangxi Province (Grant No. YC2023-S028). The authors would also like to thank Dr. Lei Xu (Nottingham Trent University) for his guidance on the nonlinear simulations.

[1] R. W. Boyd, *Nonlinear Optics* (Academic Press, New York, 2020).

[2] G. Li, S. Zhang, and T. Zentgraf, Nonlinear photonic metasurfaces, Nat. Rev. Mater. **2**, 17010 (2017).

[3] A. Krasnok, M. Tymchenko, and A. Alù, Nonlinear metasurfaces: A paradigm shift in nonlinear optics, Mater. Today **21**, 8 (2018).

[4] M. Kauranen and A. V. Zayats, Nonlinear plasmonics, Nat. Photon. **6**, 737 (2012).

[5] N. C. Panoiu, W. E. I. Sha, D. Y. Lei, and G.-C. Li, Nonlinear optics in plasmonic nanostructures, J. Opt. **20**, 083001 (2018).

[6] B. Sain, C. Meier, and T. Zentgraf, Nonlinear optics in all-dielectric nanoantennas and metasurfaces: A review, Adv. Photon. **1**, 024002 (2019).

[7] G. Grinblat, Nonlinear dielectric nanoantennas and metasurfaces: Frequency conversion and wavefront control, ACS Photon. **8**, 3406 (2021).

[8] T. Liu, S. Xiao, B. Li, M. Gu, H. Luan, and X. Fang, Third- and second-harmonic generation in all-dielectric nanostructures: A mini review, Front. Nanotechnol. **4**, 891892 (2022).

[9] C. W. Hsu, B. Zhen, A. D. Stone, J. D. Joannopoulos, and M. Soljačić, Bound states in the continuum, Nat. Rev. Mater. **1**, 16048 (2016).

[10] L. Huang, L. Xu, D. A. Powell, W. J. Padilla, and A. E. Miroshnichenko, Resonant leaky modes in all-dielectric metasystems: Fundamentals and applications, Phys. Rep. **1008**, 1 (2023).

[11] P. P. Vabishchevich, S. Liu, M. B. Sinclair, G. A. Keeler, G. M. Peake, and I. Brener, Enhanced second-harmonic generation using broken symmetry III–V semiconductor Fano metasurfaces, ACS Photon. **5**, 1685 (2018).

[12] L. Carletti, K. Koshelev, C. De Angelis, and Y. Kivshar, Giant nonlinear response at the nanoscale driven by bound states in the continuum, Phys. Rev. Lett. **121**, 033903 (2018).

[13] T. Ning, X. Li, Z. Zhang, Y. Huo, Q. Yue, L. Zhao, and Y. Gao, Ultimate conversion efficiency of second harmonic generation in all-dielectric resonators of quasi-BICs in consideration of nonlinear refraction of dielectrics, Opt. Express **29**, 17286 (2021).

[14] S. Cai, S. Zong, X. Liu, G. Liu, J. Chen, and Z. Liu, Efficiently spatial field localization enabled second-harmonic and sum-frequency generation in an etchless $LiNbO_3$ layer by guided resonant quasi-bound states in the continuum, Appl. Phys. Lett. **123**, 111701 (2023).

[15] Z. Liu, Y. Xu, Y. Lin, J. Xiang, T. Feng, Q. Cao, J. Li, S. Lan, and J. Liu, High-*Q* quasibound states in the continuum for nonlinear metasurfaces, Phys. Rev. Lett. **123**, 253901 (2019).

[16] L. Xu, K. Zangeneh Kamali, L. Huang, M. Rahmani, A. Smirnov, R. Camacho-Morales, Y. Ma, G. Zhang, M. Woolley, D. Neshev, and A. E. Miroshnichenko, Dynamic nonlinear image tuning through magnetic dipole quasi-BIC ultrathin resonators, Adv. Sci. **6**, 1802119 (2019).

[17] K. Koshelev, Y. Tang, K. Li, D.-Y. Choi, G. Li, and Y. Kivshar, Nonlinear metasurfaces governed by bound states in the continuum, ACS Photon. **6**, 1639 (2019).

[18] L. Carletti, S. S. Kruk, A. A. Bogdanov, C. De Angelis, and Y. Kivshar, High-harmonic generation at the nanoscale boosted by bound states in the continuum, Phys. Rev. Res. **1**, 023016 (2019).

[19] G. Zograf, K. Koshelev, A. Zalogina, V. Korolev, R. Hollinger, D.-Y. Choi, M. Zuerch, C. Spielmann, B. Luther-Davies, D. Kartashov, S. V. Makarov, S. S. Kruk, and Y. Kivshar, High-harmonic generation from resonant dielectric metasurfaces empowered by bound states in the continuum, ACS Photon. **9**, 567 (2022).

[20] S. Xiao, M. Qin, J. Duan, F. Wu, and T. Liu, Polarization-controlled dynamically switchable high-harmonic generation from all-dielectric metasurfaces governed by dual bound states in the continuum, Phys. Rev. B **105**, 195440 (2022).

[21] A. Zalogina, L. Carletti, A. Rudenko, J. V. Moloney, A. Tripathi, H.-C. Lee, I. Shadrivov, H.-G. Park, Y. Kivshar, and S. S. Kruk, High-harmonic generation from a subwavelength dielectric resonator, Sci. Adv. **9**, eadg2655 (2023).

[22] R. Camacho-Morales, L. Xu, H. Zhang, S. T. Ha, L. Krivitsky, A. I. Kuznetsov, M. Rahmani, and D. Neshev, Sum-frequency generation in high-Q gap metasurfaces driven by leaky-wave guided modes, Nano Lett. **22**, 6141 (2022).

[23] J. Zhang, J. Ma, M. Parry, M. Cai, R. Camacho-Morales, L. Xu, D. N. Neshev, and A. A. Sukhorukov, Spatially entangled photon pairs from lithium niobate nonlocal metasurfaces, Sci. Adv. **8**, 30 (2022).

[24] S. Feng, T. Liu, W. Chen, F. Wu, and S. Xiao, Enhanced sum-frequency generation from etchless lithium niobate empowered by dual quasi-bound states in the continuum, Sci. China Phys. Mech. Astron. **66**, 124214 (2023).

[25] T. Liu, M. Qin, S. Feng, X. Tu, T. Guo, F. Wu, and S. Xiao, Efficient photon-pair generation empowered by dual quasibound states in the continuum, Phys. Rev. B **109**, 155424 (2024).

[26] L. Xu, D. A. Smirnova, R. Camacho-Morales, R. A. Aoni, K. Z. Kamali, M. Cai, C. Ying, Z. Zheng, A. E. Miroshnichenko, D. N. Neshev, and M. Rahmani, Enhanced four-wave mixing from multi-resonant silicon dimer-hole membrane metasurfaces, New J. Phys. **24**, 035002 (2022).

[27] T. Liu, M. Qin, F. Wu, and S. Xiao, High-efficiency optical frequency mixing in an all-dielectric metasurface enabled by multiple bound states in the continuum, Phys. Rev. B **107**, 075441 (2023).

[28] G. Sanderson, Z. Zheng, E. Melik-Gaykazyan, G. S. D. Gordon, R. Cousins, C. Ying, M. Rahmani, and L. Xu, Infrared imaging with nonlinear silicon resonator governed by high-Q quasi-BIC states, J. Opt. **26**, 065505 (2024).

[29] G. Q. Moretti, T. Weber, T. Possmayer, E. Cortés, L. d. S. Menezes, A. V. Bragas, S. A. Maier, A. Tittl, and G. Grinblat, Si metasurface supporting multiple quasi-BICs for degenerate four-wave mixing, Nanophotonics (2024).

[30] R. Camacho-Morales, M. Rahmani, S. Kruk, L. Wang, L. Xu, D. A. Smirnova, A. S. Solntsev, A. Miroshnichenko, H. H. Tan, F. Karouta, S. Naureen, K. Vora, L. Carletti, C. De Angelis, C. Jagadish, Y. S. Kivshar, and D. N. Neshev, Nonlinear generation of vector beams from AlGaAs nanoantennas, Nano Lett. **16**, 7191 (2016).

[31] D. Rocco, A. Locatelli, L. Carletti, M. A. Vincenti, and C. De Angelis, Nonlinear asymmetric imaging with AlGaAs metasurface, Opt. Express **32**, 11673 (2024).

[32] See Supplemental Material at http://link.aps.org/supplemental/10.1103/PhysRevA.109.063522 for the refractive index of AlGaAs, the eigenmode analysis of quasi-BICs, the multipole decomposition, and the modeling methodology of nonlinear simulations.

[33] S. Gehrsitz, F. K. Reinhart, C. Gourgon, N. Herres, A. Vonlanthen, and H. Sigg, The refractive index of $Al_xGa_{1-x}As$ below the band gap: Accurate determination and empirical modeling, J. Appl. Phys. **87**, 7825 (2000).

[34] K. Koshelev, S. Lepeshov, M. Liu, A. Bogdanov, and Y. Kivshar, Asymmetric metasurfaces with high-*Q* resonances governed by bound states in the continuum, Phys. Rev. Lett. **121**, 193903 (2018).

[35] Y. Gao, L. Xu, and X. Shen, Q-factor mediated quasi-BIC resonances coupling in asymmetric dimer lattices, Opt. Express **30**, 46680 (2022).

[36] W. Ma and C. Zhou, Quasi-symmetry-protected BICs in a double-notched silicon nanodisk metasurface, Opt. Lett. **48**, 2158 (2023).

[37] S. Xiao, T. Liu, X. Wang, X. Liu, and C. Zhou, Tailoring the absorption bandwidth of graphene at critical coupling, Phys. Rev. B **102**, 085410 (2020).

[38] X. Wang, J. Duan, W. Chen, C. Zhou, T. Liu, and S. Xiao, Controlling light absorption of graphene at critical coupling through magnetic dipole quasi-bound states in the continuum resonance, Phys. Rev. B **102**, 155432 (2020).

[39] T. Kaelberer, V. A. Fedotov, N. Papasimakis, D. P. Tsai, and N. I. Zheludev, Toroidal dipolar response in a metamaterial, Science **330**, 1510 (2010).

[40] V. Savinov, V. A. Fedotov, and N. I. Zheludev, Toroidal dipolar excitation and macroscopic electromagnetic

properties of metamaterials, Phys. Rev. B **89**, 205112 (2014).

[41] B. E. Saleh and M. C. Teich, *Fundamentals of Photonics* (Wiley, Hoboken, 2019).

[42] I. Volkovskaya, L. Xu, L. Huang, A. I. Smirnov, A. E. Miroshnichenko, and D. Smirnova, Multipolar second-harmonic generation from high-Q quasi-BIC states in subwavelength resonators, Nanophotonics **9**, 3953 (2020).

[43] D. Rocco, L. Carletti, R. Caputo, M. Finazzi, M. Celebrano, and C. De Angelis, Switching the second harmonic generation by a dielectric metasurface via tunable liquid crystal, Opt. Express **28**, 12037 (2020).

[44] Q. Yang, Y. Liu, X. Gan, C. Fang, G. Han, and Y. Hao, Nonlinear bound states in the continuum of etchless lithium niobate metasurfaces, IEEE Photon. J. **12**, 4601209 (2020).

[45] Y. Gao, Y. Fan, Y. Wang, W. Yang, Q. Song, and S. Xiao, Nonlinear holographic all-dielectric metasurfaces, Nano Lett. **18**, 8054 (2018).

[46] F. Timpu, M. Reig Escalé, M. Timofeeva, N. Strkalj, M. Trassin, M. Fiebig, and R. Grange, Enhanced nonlinear yield from barium titanate metasurface down to the near ultraviolet, Adv. Opt. Mater. **7**, 1900936 (2019).

[47] S. Liu, M. B. Sinclair, S. Saravi, G. A. Keeler, Y. Yang, J. Reno, G. M. Peake, F. Setzpfandt, I. Staude, T. Pertsch, and I. Brener, Resonantly enhanced second-harmonic generation using III–V semiconductor all-dielectric metasurfaces, Nano Lett. **16**, 5426 (2016).

[48] V. F. Gili, L. Carletti, A. Locatelli, D. Rocco, M. Finazzi, L. Ghirardini, I. Favero, C. Gomez, A. Lemaître, M. Celebrano, C. De Angelis, and G. Leo, Monolithic AlGaAs second-harmonic nanoantennas, Opt. Express **24**, 15965 (2016).